Advances in Aircraft and Spacecraft Science, *Vol. 9, No. 3 (2022) 169-193*
https://doi.org/10.12989/aas.2022.9.3.169

Vibration behavior of partially bio-sourced sandwich panel with orthogonally stiffened core: Analytical and experiment study

Aicha Boussoufi[1a], Lahouaria Errouane[1], Zouaoui Sereir*[1], José V. Antunes[2] and Vincent Debut[2]

[1]Laboratoire Structures des Composites et MatériauxInnovants, Department of Marine Engineering, University of Science and Technology of Oran, BP 1505 El M'naouer USTO, Oran, Algeria
[2]Applied Dynamics Laboratory, Instituto Technològico e Nuclear, ITN/ADL, Estrada Nacional 10, 2686 Sacavem Codex, Portugal

(Received January 13, 2022, Revised April 2, 2022, Accepted April 6, 2022)

Abstract. By the present paper, both experimental and analytical models have been proposed to study the vibration behavior of partially bio-sourced sandwich panel with orthogonally stiffened core. For a variable mass fraction of Alfa fibers from 5% to 15%, impregnated in a Medapoxy STR resin, this panel were manufactured by molding the orthogonally stiffened core then attached it with both skins. Using simply supported boundary conditions, a free vibration test was carried out using an impact hammer for predicting the natural frequencies, the mode shapes and the damping coefficient versus the fibers content. In addition, an analytical model based on the Higher order Shear Deformation Theory (HSDT) was developed to predict natural frequencies and the mode shapes according to Navier's solution. From the experimental test, we have found that the frequency increases with the increase in the mass fraction of the fibers until 10%. Beyond this fraction, the frequencies give relatively lower values. For the analytical model, variation of the natural frequencies increased considerably with side-to-thickness ratio (a/H) and equivalent thickness of the core to thickness of the face (h_s/h). We concluded that, the vibration behavior was significantly influenced by geometrical and mechanical properties of the partially bio-sourced sandwich panel.

Keywords: equivalent stiffness; orthogonally stiffeners; sandwich panel; short Alfa fibers; vibration behavior

1. Introduction

Orthogonally stiffened sandwich structures obtained by the assembly of the orthogrid core placed between two face sheets, are usually used in several engineering fields such as automobile, building constructions, aircrafts and shipbuilding. The best advantage of sandwich panels is that optimal designs enables us to have large bending stiffness, low structural mass and significant flexibility to adapt different properties reaching strength and stiffness requirements. In addition, it allows changing the natural frequencies and its mode shapes by adding stiffeners instead of increasing the

*Corresponding author, Professor, E-mail: serzou@hotmail.com
[a]Ph.D. Student, E-mail: aicha.boussoufi@univ-usto.dz

http://www.techno-press.org/?journal=aas&subpage=7 ISSN: 2287-528X (Print), 2287-5271 (Online)

thickness of the panel, which also reduces the cost and the damage probability (Liu and Jeffers 2017a, b, Khaldi *et al.* 2016, Teo *et al*. 2016, Hamamousse *et al*. 2019, Benzidane *et al*. 2018, Merzoug *et al*.2020).

Therefore, several analytical models have been devoted to predicting the natural frequencies of stiffened sandwich panels. Most part of these models used either the HSDT because the Classical Laminate Plate theory (CLPT) ignores the effect of transverse shear deformation and the First-order Shear deformation Theory (FSDT) considers the constant states of the transverse shear stress requiring the correction coefficients. In this way, Kant and Swaminathan (2001) developed a dynamic behavior of sandwich plates based on the HSDT. They applied Hamilton's principle to have the equations of the motion and the significant natural frequencies of simply supported sandwich plates. The results showed the accuracy of the HSDT in prediction of the natural frequencies. Wang and Wang (2015) used the weak form quadrature element method to analyze the free vibration of sandwich beams. He found that a beam element can give very precise frequencies with a relatively small number of nodes. The prediction of the sandwich plate's natural frequencies using new shear deformable dynamic stiffness elements was proposed by Marjanović *et al*. (2016). Using a zigzag in-plane displacements distribution and HSDT, Phan *et al*. (2013) studied the free vibration response of a sandwich panel with an incompressible core. The models adopted an approach which substitutes the layered sandwich panel with a one layer only with equivalent geometric and mechanical properties. Liu *et al*. (2018) employed B-spline basis functions to define the deformation along the length, while a layer-based through-the-thickness discretization is adopted to capture the gradual plastification of the isogeometric frame. After that (Lieu *et al*. 2018), they used the high-order smooth basis functions also alleviates shear and membrane locking phenomena that commonly occurred in shell structures.

As for periodically stiffened plates sandwich structure, there are many methods which have studied their dynamic behavior using mathematical developments simplifying the stiffeners shape. Thus, the replacement of orthogonally stiffened panels by an equivalent orthotropic sandwich plate of constant thickness is appropriate, when the ribs are disposed symmetrically. Using an harmonic force excitation, Xin and Lu (2011) theoretically formulated the wave propagation in the sandwich panel reinforced by orthogonal rib-stiffeners. In order to optimize the low-frequency sound radiation of an orthogonally rib-stiffened sandwich structure, the cyclic sub wave length of piezoelectric patches were introduced by Zhang *et al*. (2018). All the results demonstrate that the proposed structure can effectively attenuate the structural radiation. Fu *et al*. (2018) developed an analytical model to study the sound propagation in orthogonally rib-stiffened sandwich structures. More recently, the vibration of a sandwich panel with a honeycomb core has been investigated by Petrolo *et al*. (2016).

From literature, a limited experimental validation and testing procedures are available to examine the accuracy of numerical models and to characterize the modal behavior of stiffened panel. For that, some measurement techniques are described in detail in references by Petrone *et al*. (2017), Teo *et al*. (2016), Thinhand Quoc (2016), Sahoo *et al*. (2017), Ehsani and Rezaeepazhand (2016), Xu *et al*. (2019). Sinha *et al*. (2020) proposed both numerical and experimental models to study the free vibration of woven glass fiber laminated composite stiffened plates. To obtain a stiff, weight and strong cylindrical shell, Jiang *et al*. (2017) fabricated and vibration tested a carbon fiber reinforced orthogrid-cores and cylinder. In addition, free vibration of cylindrical sandwich shells with orthogonally rib-stiffened core was investigated experimentally and numerically by Shahgholian-Ghahfarokhi *et al*. (2020). Modal test was performed, and natural frequencies were predicted. Sandwich panels by a grid-stiffened core were fabricated to measure the damping

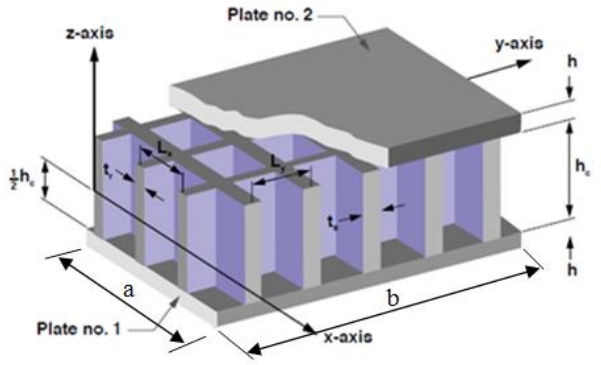

Fig. 1 Design and coordinates of the orthogrid sandwich panel (Nemeth 2011)

coefficients, natural frequencies and mode shapes (Azarafza *et al*. 2018). They noted that, with increasing frequency, the mode changed from the bending type to the twisting type due to the increased overall stiffness at the specified frequency.

From the literature it has been noticed that a wide field of application for performing natural frequency measurements of stiffened panels reinforced with synthetic fibers, but very few have based on the analytical-experimental vibration analysis of stiffened sandwich panels reinforced by natural fibers. Moreover, the previous experimental studies considered only the clamped or free boundary conditions. Using a simply supported edges boundary conditions, a significant effort has been made to investigate vibration behavior of the partially bio-sourced sandwich panel with orthogonally stiffened core. This mode fixation is not easy to achieve due to the rigid-body modes. To achieve this aim, the panel was manufactured by molding the orthogonally stiffened core then assembling it with both skins according to the variable mass fraction of Alfa short fibers from 5% to 15%. Using a Fast Fourier Transform (FFT) Analyzer, natural frequencies, mode shapes and damping factors were predicted for each mass fraction of Alfa fibers. Using a new simplified orthogonal model based on the equivalent element, an analytical model based on the HSDT was developed to predict fundamental frequencies and the mode shapes according to Navier's solution. Since no existing results of Orthogonally Stiffened Sandwich Structures reinforced with short Alfa fibers, comparison studies can only be made with the sandwich panels reinforced with synthetic fibers. In addition, a comparison was made also between the developed analytical and experimental models. Looking at the small difference between the analytical model and the experimental results for the three first natural frequencies and the literature results, it is possible to confirm that a good agreement was found from these comparative studies. In terms of frequency response, a parametric study was performed in order to investigate the effect of different percentage of Alfa Fibers in the core and faces, as well as the effect of the random distribution of the fibers and geometric ratios of the sandwich panel.

2. Analytical model: Level 1

2.1 Equivalent stiffnesses of the sandwich panel

In this section, we attempt to find the equivalent plate thickness from the orthogrid sandwich

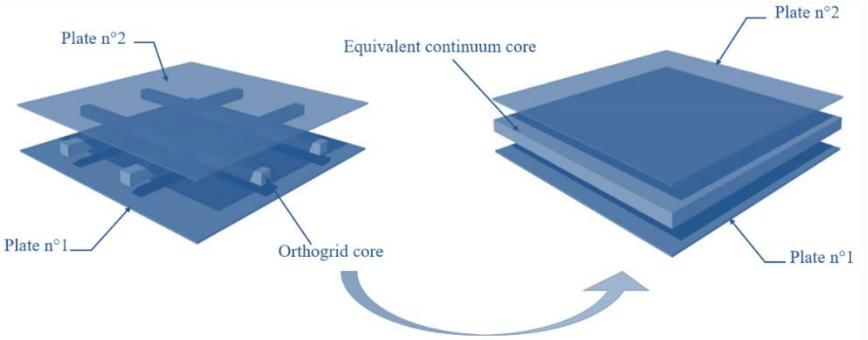

(a) The design parameters of sandwich plate with orthogrid core

(b) The equivalent continuum sandwich plate

Fig. 2 The sandwich plate with orthogrid core, (a) the design parameters of sandwich plate with orthogrid core, (b) the equivalent continuum sandwich plate

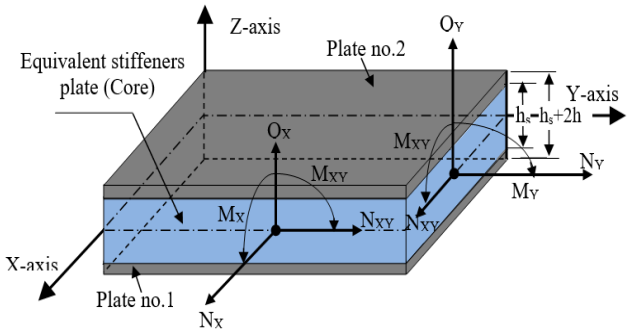

Fig. 3 Resultant forces and moments in the equivalent sandwich plate

panel. The orthogrid sandwich plate shown in Fig. 1 has a regular orthogrid core with the same layout as the stiffening arrangement. The stringer and rib elements of the core are aligned with the *x*- and *y*-axes with spacing's L_x and L_y. t_r and t_s are the core wall thicknesses of sandwich plate, respectively. The equivalent-plate thickness for a sandwich panel composed by two faces and the orthogrid core was shown in Fig. 2. The thicknesses of the bottom face plate, the top face plate and the core were denoted by h= and h_c, respectively. Member associated with the ribs and stringers are denoted by subscripts or superscripts «*r*» and «*s*», respectively.

To have the equivalent thickness of the orthogrid core, the stiffened-plate cell is modeled as the equivalent-plate given by Fig. 3. Both skins are perfectly bonded to an equivalent-stiffener layer. Then, the equivalent plate thickness $2h+h_s$ is given in Fig. 3. According to the reference, the equivalent-stiffener layer, is given by (Semmani *et al*. 2020)

$$\int_0^{d_s} \int_{-\frac{h_s}{2}}^{\frac{h_s}{2}} Z^2 dYdZ = I_{YY}^s \tag{1}$$

From this integral, we have the equivalent thickness of the plate.

$$h_s = \sqrt[3]{\frac{12 I_{YY}^s}{d_s}} \tag{2}$$

Where I_{YY}^{S} denote the inertia moment of stiffeners.

To develop the stiffness of the equivalent plate in HSDT, we will use the same methodology as that used in Nemeth (2011), Semmani *et al*. (2020) and Reddy (2003). Except, that we will have to relax the hypothesis on the straightness and normality of a transverse normal after deformation. The HSDT was used because it takes in consideration the geometric non-linearity present in the thick sandwich beams.

For this, we have adopted cubic functions of displacements (u, v) through the thickness. However, the transverse displacement component w was supposed constant through the plate thickness (Reddy 2003, Whitney and Pagano 1970)

$$\begin{aligned} u(x,y,z) &= u_0(x,y) + z\theta_x(x,y) + z^2 u_0^*(x,y) + z^3\theta_x^*(x,y) \\ v(x,y,z) &= v_0(x,y) + z\theta_y(x,y) + z^2 v_0^*(x,y) + z^3\theta_y^*(x,y) \\ w(x,y,z) &= w_0(x,y) \end{aligned} \tag{3}$$

Where u_0, v_0 and w_0 denote the in-plane and the transverse displacement at the midplane. θ_x, θ_y denote the rotations of the normal to the midplane about y and x-axis, respectively.

u_0^*, v_0^*, θ_x^* and θ_y^* are the higher order transverse deformation modes.

By substitution of these displacement relations into the strain-deformation equations of the Classical Laminated Plate Theory (CLTP), we obtained (Reddy 2003).

$$\begin{Bmatrix} \varepsilon_x \\ \varepsilon_y \\ \gamma_{xy} \end{Bmatrix} = \begin{Bmatrix} \varepsilon_{x0} \\ \varepsilon_{y0} \\ \gamma_{xy0} \end{Bmatrix} + z\begin{Bmatrix} k_x \\ k_y \\ k_{xy} \end{Bmatrix} + z^2\begin{Bmatrix} \varepsilon_{x0}^* \\ \varepsilon_{y0}^* \\ \gamma_{xy0}^* \end{Bmatrix} + z^3\begin{Bmatrix} k_x^* \\ k_y^* \\ k_{xy}^* \end{Bmatrix} \tag{4}$$

$$\begin{Bmatrix} \gamma_{yz} \\ \gamma_{xz} \end{Bmatrix} = \begin{Bmatrix} \phi_y \\ \phi_x \end{Bmatrix} + z\begin{Bmatrix} k_{yz} \\ k_{xz} \end{Bmatrix} + z^2\begin{Bmatrix} \phi_y^* \\ \phi_x^* \end{Bmatrix} \tag{5}$$

Where

$$(\varepsilon_{x0}, \varepsilon_{y0}, \varepsilon_{xy0}) = \left(\frac{\partial u_0}{\partial x}, \frac{\partial v_0}{\partial y}, \frac{\partial u_0}{\partial y} + \frac{\partial v_0}{\partial x}\right), (\varepsilon_{x0}^*, \varepsilon_{y0}^*, \varepsilon_{xy0}^*) = \left(\frac{\partial u_0^*}{\partial x}, \frac{\partial v_0^*}{\partial y}, \frac{\partial u_0^*}{\partial y} + \frac{\partial v_0^*}{\partial x}\right),$$

$$(k_x, k_y, k_{xy}) = \left(\frac{\partial \theta_x}{\partial x}, \frac{\partial \theta_y}{\partial y}, \frac{\partial \theta_x}{\partial y} + \frac{\partial \theta_y}{\partial x}\right), (k_{xz}, k_{yz}) = (2u_0^*, 2v_0^*),$$

$$(k_x^*, k_y^*, k_{xy}^*) = \left(\frac{\partial \theta_x^*}{\partial x}, \frac{\partial \theta_y^*}{\partial y}, \frac{\partial \theta_x^*}{\partial y} + \frac{\partial \theta_y^*}{\partial x}\right), (\phi_x, \phi_x^*, \phi_y, \phi_y^*) = \left(\theta_x + \frac{\partial w_0}{\partial x}, 3\theta_x^*, \theta_y + \frac{\partial w_0}{\partial y}, 3\theta_y^*\right).$$

where $(\varepsilon_{x0}, \varepsilon_{y0}, \varepsilon_{xy0})$, $(\varepsilon_{x0}^*, \varepsilon_{y0}^*, \varepsilon_{xy0}^*)$, (k_x, k_y, k_{xy}), (k_{xz}, k_{yz}), (k_x^*, k_y^*, k_{xy}^*) and $(\phi_x, \phi_x^*, \phi_y, \phi_y^*)$ areusual deformations, curvatures and rotations involved by CLTP and HSDT theories(Kant and Swaminathan 2001 and Reddy (2003)).

According to HSDT, normal forces (N_x, N_y, N_{xy}), (N_x^*, N_y^*, N_{xy}^*), shear forces (Q_x, Q_y), (Q_x^*, Q_y^*), (S_x, S_y) and moments (M_x, M_y, M_{xy}), (M_x^*, M_y^*, M_{xy}^*) resultants are given by:

$$\begin{bmatrix} N_x & N_x^* \\ N_y & N_y^* \\ N_{xy} & N_{xy}^* \end{bmatrix} = \sum_{L=1}^{NL} \int_{z_L}^{z_{L+1}} \begin{Bmatrix} \sigma_x \\ \sigma_y \\ \tau_{xy} \end{Bmatrix} \begin{bmatrix} 1 & z^2 \end{bmatrix} dz \tag{6}$$

$$\begin{bmatrix} M_x & M_x^* \\ M_y & M_y^* \\ M_{xy} & M_{xy}^* \end{bmatrix} = \sum_{L=1}^{NL} \int_{z_L}^{z_{L+1}} \begin{Bmatrix} \sigma_x \\ \sigma_y \\ \tau_{xy} \end{Bmatrix} \begin{bmatrix} z & z^3 \end{bmatrix} dz \tag{7}$$

$$\begin{bmatrix} Q_x & Q_x^* \\ Q_y & Q_y^* \end{bmatrix} = \sum_{L=1}^{NL} \int_{z_L}^{z_{L+1}} \begin{Bmatrix} \tau_{xz} \\ \tau_{yz} \end{Bmatrix} \begin{bmatrix} 1 & z^2 \end{bmatrix} dz \tag{8}$$

$$\begin{bmatrix} S_x \\ S_y \end{bmatrix} = \sum_{L=1}^{NL} \int_{z_L}^{z_{L+1}} \begin{Bmatrix} \tau_{xz} \\ \tau_{yz} \end{Bmatrix} z dz \tag{9}$$

Where $(\sigma_x, \sigma_y, \tau_{xy})$ and (τ_{xz}, τ_{yz}) are the in plane and transverse stress components related to the strain components $(\varepsilon_x, \varepsilon_y, \gamma_{xy})$ and $(\gamma_{xz}, \gamma_{yz})$ by the constitutive equation

$$\begin{Bmatrix} \sigma_x \\ \sigma_y \\ \sigma_z \\ \tau_{yz} \\ \tau_{xz} \\ \tau_{xy} \end{Bmatrix} = \begin{bmatrix} \overline{C}_{11} & \overline{C}_{12} & \overline{C}_{13} & 0 & 0 & \overline{C}_{16} \\ \overline{C}_{12} & \overline{C}_{22} & \overline{C}_{33} & 0 & 0 & \overline{C}_{26} \\ \overline{C}_{13} & \overline{C}_{23} & \overline{C}_{33} & 0 & 0 & \overline{C}_{36} \\ 0 & 0 & 0 & \overline{C}_{44} & 0 & 0 \\ 0 & 0 & 0 & 0 & \overline{C}_{55} & 0 \\ \overline{C}_{16} & \overline{C}_{26} & \overline{C}_{36} & 0 & 0 & \overline{C}_{66} \end{bmatrix} \begin{Bmatrix} \varepsilon_x \\ \varepsilon_y \\ \varepsilon_z \\ \gamma_{yz} \\ \gamma_{xz} \\ \gamma_{xy} \end{Bmatrix} \tag{10}$$

For composite material, the elastic constant of transformed stiffness matrix elements $\bar{C}_{i,j}$, are detailed in refs (Kant and Swaminathan 2001, Nemeth 2011, Semmani *et al.* 2020, Whitney and Pagano 1970, Reddy 2003). The composite material herein is made from a mixture of isotropic matrix (epoxy resin), and short Alfa fibers which are distributed randomly through the matrix. The model of Halpin (Halpin and Tsai 1969) is proposed to predict the elastic properties of partially bio-sourced composite material and to compare the Young's modulus predicted theoretically with that obtained experimentally.

$$E = E_m \left[\frac{3}{8} \left(\frac{1 + \xi \eta_L V_f}{1 - \xi \eta_L V_f} \right) + \frac{5}{8} \left(\frac{1 + 2\eta_T V_f}{1 - \eta_T V_f} \right) \right] \tag{11}$$

where

$$\eta_L = \frac{E_f / E_m - 1}{E_f / E_m + 2l_f / d_f}; \eta_T = \frac{E_f / E_m - 1}{E_f / E_m + 2}; \xi = 2l_f / d_f$$

E_f, E_m are the elastic modulus of the fiber and the matrix, respectively, V_f is the volume fraction of the fibers, l_f and d_f are length and diameter of a fiber, respectively. In the present paper (fibers are 0.1 mm to 0.5 mm in diameter and 0.86 mm to 4.5 mm in length).

Substituting Eqs. (2)-(5) in (6)-(9), the stress resultants of the sandwich panel with are detailed on the following

$$\begin{Bmatrix} N_x \\ N_y \\ N_{xy} \end{Bmatrix} = [A] \begin{Bmatrix} \varepsilon_{x0} \\ \varepsilon_{y0} \\ \varepsilon_{xy0} \end{Bmatrix} + [B] \begin{Bmatrix} k_x \\ k_y \\ k_{xy} \end{Bmatrix} + [A^*] \begin{Bmatrix} \varepsilon_{x0}^* \\ \varepsilon_{y0}^* \\ \varepsilon_{xy0}^* \end{Bmatrix} + [E] \begin{Bmatrix} k_x^* \\ k_y^* \\ k_{xy}^* \end{Bmatrix} \tag{12}$$

$$\begin{Bmatrix} N_x^* \\ N_y^* \\ N_{xy}^* \end{Bmatrix} = \begin{bmatrix} A^* \end{bmatrix} \begin{Bmatrix} \varepsilon_{x0} \\ \varepsilon_{y0} \\ \varepsilon_{xy0} \end{Bmatrix} + \begin{bmatrix} E \end{bmatrix} \begin{Bmatrix} k_x \\ k_y \\ k_{xy} \end{Bmatrix} + \begin{bmatrix} A^{**} \end{bmatrix} \begin{Bmatrix} \varepsilon_{x0}^* \\ \varepsilon_{y0}^* \\ \varepsilon_{xy0}^* \end{Bmatrix} + \begin{bmatrix} G \end{bmatrix} \begin{Bmatrix} k_x^* \\ k_y^* \\ k_{xy}^* \end{Bmatrix} \tag{13}$$

$$\begin{Bmatrix} M_x \\ M_y \\ M_{xy} \end{Bmatrix} = \begin{bmatrix} B \end{bmatrix} \begin{Bmatrix} \varepsilon_{x0} \\ \varepsilon_{y0} \\ \varepsilon_{xy0} \end{Bmatrix} + \begin{bmatrix} D \end{bmatrix} \begin{Bmatrix} k_x \\ k_y \\ k_{xy} \end{Bmatrix} + \begin{bmatrix} E \end{bmatrix} \begin{Bmatrix} \varepsilon_{x0}^* \\ \varepsilon_{y0}^* \\ \varepsilon_{xy0}^* \end{Bmatrix} + \begin{bmatrix} F \end{bmatrix} \begin{Bmatrix} k_x^* \\ k_y^* \\ k_{xy}^* \end{Bmatrix} \tag{14}$$

$$\begin{Bmatrix} M_x^* \\ M_y^* \\ M_{xy}^* \end{Bmatrix} = \begin{bmatrix} E \end{bmatrix} \begin{Bmatrix} \varepsilon_{x0} \\ \varepsilon_{y0} \\ \varepsilon_{xy0} \end{Bmatrix} + \begin{bmatrix} F \end{bmatrix} \begin{Bmatrix} k_x \\ k_y \\ k_{xy} \end{Bmatrix} + \begin{bmatrix} G \end{bmatrix} \begin{Bmatrix} \varepsilon_{x0}^* \\ \varepsilon_{y0}^* \\ \varepsilon_{xy0}^* \end{Bmatrix} + \begin{bmatrix} H \end{bmatrix} \begin{Bmatrix} k_x^* \\ k_y^* \\ k_{xy}^* \end{Bmatrix} \tag{15}$$

Where [A], [A^*], [A^{**}], [B], [D], [E], [F], [G], [H] are the stiffness's matrix of the equivalent plate. For the sandwich orthogrid panel, these matrices are obtained by algebraic sum of both skins (plate 1 and 2) and stiffeners rigidity contribution. It should be noted that this theory takes into consideration the non-symmetry of the two skins of the panel (plate 1 and 2). [A_{ij}], [B_{ij}], and [D_{ij}] (i,j=1,2,6) are named the extensional, coupling, and bending stiffness matrices, respectively. The tensile, coupling, bending, and shear stiffness matrices of the plates are given by Reissner-Mindlin type shear deformation plate theory. To obtain these matrices, we followed the same method used by Semmani *et al.* (2020) and Nemeth (2011).

$$\begin{bmatrix} A_{11} & A_{12} & A_{16} \\ A_{12} & A_{22} & A_{26} \\ A_{16} & A_{26} & A_{66} \end{bmatrix} = h^1 \begin{bmatrix} Q_{11} & Q_{12} & 0 \\ Q_{21} & Q_{22} & 0 \\ 0 & 0 & Q_{66} \end{bmatrix}^{Pl1} + h^1 \begin{bmatrix} Q_{11} & Q_{12} & 0 \\ Q_{21} & Q_{22} & 0 \\ 0 & 0 & Q_{66} \end{bmatrix}^{Pl2} + \begin{bmatrix} \dfrac{E_x{}^{core} h_c t_s}{L_y} & 0 & 0 \\ 0 & \dfrac{E_y{}^{core} h_c t_r}{L_x} & 0 \\ 0 & 0 & \dfrac{G_{xy}{}^{core} h_c t_s}{4L_y} + \dfrac{G_{xy}^{core} h_c t_r}{4L_x} \end{bmatrix} \tag{16}$$

$$\begin{bmatrix} B_{11} & B_{12} & B_{16} \\ B_{12} & B_{22} & B_{26} \\ B_{16} & B_{26} & B_{66} \end{bmatrix} = h^2 \begin{bmatrix} Q_{11} & Q_{12} & 0 \\ Q_{21} & Q_{22} & 0 \\ 0 & 0 & Q_{66} \end{bmatrix}^{Pl1} + h^2 \begin{bmatrix} Q_{11} & Q_{12} & 0 \\ Q_{21} & Q_{22} & 0 \\ 0 & 0 & Q_{66} \end{bmatrix}^{Pl2} \tag{17}$$

$$\begin{bmatrix} D_{11} & D_{12} & D_{16} \\ D_{12} & D_{22} & D_{26} \\ D_{16} & D_{26} & D_{66} \end{bmatrix} = h^3 \begin{bmatrix} Q_{11} & Q_{12} & 0 \\ Q_{21} & Q_{22} & 0 \\ 0 & 0 & Q_{66} \end{bmatrix}^{Pl1} + h^3 \begin{bmatrix} Q_{11} & Q_{12} & 0 \\ Q_{21} & Q_{22} & 0 \\ 0 & 0 & Q_{66} \end{bmatrix}^{Pl2} + \begin{bmatrix} \dfrac{E_x{}^{core} h_c{}^3 t_s}{12L_y} & 0 & 0 \\ 0 & \dfrac{E_y{}^{core} h_c{}^3 t_r}{12L_x} & 0 \\ 0 & 0 & \dfrac{h_c}{12}\left(\dfrac{G_{xz}{}^{core} t_s{}^3 (1-K_s)}{L_y} + \dfrac{G_{yz}^{core} t_r{}^3 (1-K_r)}{L_x} \right) \end{bmatrix}^{core} \tag{18}$$

Where

$$K_r = \frac{96}{\pi^5}\frac{t_r}{h_c}\left(\frac{G_{xz}^{core}}{G_{xy}^{core}}\right)^{\frac{1}{2}}\sum_{p=1,2,3,..}^{\infty}\left[\frac{1-(-1)^p}{p^5}\tanh\left(\frac{p\pi h_c}{2t_r}\left(\frac{G_{xy}^{core}}{G_{xz}^{core}}\right)^{\frac{1}{2}}\right)\right]$$

$$K_s = \frac{96}{\pi^5}\frac{t_s}{h_c}\left(\frac{G_{xz}^{core}}{G_{xy}^{core}}\right)^{\frac{1}{2}}\sum_{p=1,2,3,..}^{\infty}\left[\frac{1-(-1)^p}{p^5}\tanh\left(\frac{p\pi h_c}{2t_s}\left(\frac{G_{xy}^{core}}{G_{xz}^{core}}\right)^{\frac{1}{2}}\right)\right]$$

Note that the high order developed stiffnesses [A^*], [A^{**}], [E], [F], [G] and [H] involving higher powers of the thickness of skins (h^i, i=1, 7) are given by

$$\begin{bmatrix} A_{11}^* & A_{12}^* & A_{16}^* \\ A_{12}^* & A_{22}^* & A_{26}^* \\ A_{16}^* & A_{26}^* & A_{66}^* \end{bmatrix} = h^3\begin{bmatrix} Q_{11} & Q_{12} & 0 \\ Q_{21} & Q_{22} & 0 \\ 0 & 0 & Q_{66} \end{bmatrix}^{Pl1} + h^3\begin{bmatrix} Q_{11} & Q_{12} & 0 \\ Q_{21} & Q_{22} & 0 \\ 0 & 0 & Q_{66} \end{bmatrix}^{pl2}$$
$$+\begin{bmatrix} \frac{E_x{}^{core}h_c^3t_s}{12L_y} & 0 & 0 \\ 0 & \frac{E_y{}^{core}h_c^3t_r}{12L_x} & 0 \\ 0 & 0 & \frac{G_{xy}{}^{core}h_c^3t_s}{12L_y}+\frac{G_{xy}^{core}h_c^3t_r}{12L_x} \end{bmatrix}^{core} \tag{19}$$

$$\begin{bmatrix} A_{11}^{**} & A_{12}^{**} & A_{16}^{**} \\ A_{12}^{**} & A_{22}^{**} & A_{26}^{**} \\ A_{16}^{**} & A_{26}^{**} & A_{66}^{**} \end{bmatrix} = h^5\begin{bmatrix} Q_{11} & Q_{12} & 0 \\ Q_{21} & Q_{22} & 0 \\ 0 & 0 & Q_{66} \end{bmatrix}^{Pl1} + h^5\begin{bmatrix} Q_{11} & Q_{12} & 0 \\ Q_{21} & Q_{22} & 0 \\ 0 & 0 & Q_{66} \end{bmatrix}^{Pl2}$$
$$+\begin{bmatrix} \frac{E_x{}^{core}h_c^5t_s}{80L_y} & 0 & 0 \\ 0 & \frac{E_y{}^{core}h_c^5t_r}{80L_x} & 0 \\ 0 & 0 & \frac{G_{xy}{}^{core}h_c^5t_s}{320L_y}+\frac{G_{xy}^{core}h_c^5t_r}{320L_x} \end{bmatrix}^{core} \tag{20}$$

$$\begin{bmatrix} E_{11} & E_{12} & E_{16} \\ E_{12} & E_{22} & E_{26} \\ E_{16} & E_{26} & E_{66} \end{bmatrix} = h^4\begin{bmatrix} Q_{11} & Q_{12} & 0 \\ Q_{21} & Q_{22} & 0 \\ 0 & 0 & Q_{66} \end{bmatrix}^{Pl1} + h^4\begin{bmatrix} Q_{11} & Q_{12} & 0 \\ Q_{21} & Q_{22} & 0 \\ 0 & 0 & Q_{66} \end{bmatrix}^{Pl2} \tag{21}$$

$$\begin{bmatrix} F_{11} & F_{12} & F_{16} \\ F_{12} & F_{22} & F_{26} \\ F_{16} & F_{26} & F_{66} \end{bmatrix} = h^5\begin{bmatrix} Q_{11} & Q_{12} & 0 \\ Q_{21} & Q_{22} & 0 \\ 0 & 0 & Q_{66} \end{bmatrix}^{P1} + h^5\begin{bmatrix} Q_{11} & Q_{12} & 0 \\ Q_{21} & Q_{22} & 0 \\ 0 & 0 & Q_{66} \end{bmatrix}^{pl2}$$
$$+\begin{bmatrix} \frac{E_x{}^{core}h_c{}^5t_s}{80L_y} & 0 & 0 \\ 0 & \frac{E_y{}^{core}h_c{}^5t_r}{80L_x} & 0 \\ 0 & 0 & \frac{h_c}{20}\left(\frac{G_{xz}{}^{core}t_s{}^5(1-K_s^*)}{L_y}+\frac{G_{yz}^{core}t_r{}^5(1-K_r^*)}{L_x}\right) \end{bmatrix}^{core} \tag{22}$$

$$\begin{bmatrix} G_{11} & G_{12} & G_{16} \\ G_{12} & G_{22} & G_{26} \\ G_{16} & G_{26} & G_{66} \end{bmatrix} = h^6 \begin{bmatrix} Q_{11} & Q_{12} & 0 \\ Q_{21} & Q_{22} & 0 \\ 0 & 0 & Q_{66} \end{bmatrix}^{Pl1} + h^6 \begin{bmatrix} Q_{11} & Q_{12} & 0 \\ Q_{21} & Q_{22} & 0 \\ 0 & 0 & Q_{66} \end{bmatrix}^{Pl2} \tag{23}$$

$$\begin{bmatrix} H_{11} & H_{12} & H_{16} \\ H_{12} & H_{22} & H_{26} \\ H_{16} & H_{26} & H_{66} \end{bmatrix} = h^7 \begin{bmatrix} Q_{11} & Q_{12} & 0 \\ Q_{21} & Q_{22} & 0 \\ 0 & 0 & Q_{66} \end{bmatrix}^{Pl1} + h^7 \begin{bmatrix} Q_{11} & Q_{12} & 0 \\ Q_{21} & Q_{22} & 0 \\ 0 & 0 & Q_{66} \end{bmatrix}^{Pl2}$$
$$+ \begin{bmatrix} \frac{E_x{}^{core} h_c{}^7 t_s}{448 L_y} & 0 & 0 \\ 0 & \frac{E_y{}^{core} h_c{}^7 t_r}{448 L_x} & 0 \\ 0 & 0 & \frac{h_c}{28}\left(\frac{G_{xz}{}^{core} t_s{}^7 (1-K_s^+)}{L_y} + \frac{G_{yz}^{core} t_r{}^7 (1-K_r^+)}{L_x} \right) \end{bmatrix}^{core} \tag{24}$$

Where

$$K_s^* = \frac{160}{\pi^5}\left(\frac{t_s}{h_c}\right)^2 \left(\frac{G_{xz}^{core}}{G_{xy}^{core}}\right)^{\frac{1}{2}} \sum_{p=1,2,3,..}^{\infty} \left[\frac{(1-(-1)^p)^2}{p^5} \tanh\left(\frac{p\pi h_c^2}{4t_s^2} \left(\frac{G_{xy}^{core}}{G_{xz}^{core}} \right)^{\frac{1}{2}} \right) \right]$$

$$K_r^* = \frac{160}{\pi^5}\left(\frac{t_r}{h_c}\right)^2 \left(\frac{G_{xz}^{core}}{G_{xy}^{core}}\right)^{\frac{1}{2}} \sum_{p=1,2,3,..}^{\infty} \left[\frac{(1-(-1)^p)^2}{p^5} \tanh\left(\frac{p\pi h_c^2}{4t_r^2} \left(\frac{G_{xy}^{core}}{G_{xz}^{core}} \right)^{\frac{1}{2}} \right) \right]$$

$$K_s^+ = \frac{224}{\pi^5}\left(\frac{t_s}{h_c}\right)^3 \left(\frac{G_{xz}^{core}}{G_{xy}^{core}}\right)^{\frac{1}{2}} \sum_{p=1,2,3,..}^{\infty} \left[\frac{(1-(-1)^p)^3}{p^5} \tanh\left(\frac{p\pi h_c^3}{8t_s^3} \left(\frac{G_{xy}^{core}}{G_{xz}^{core}} \right)^{\frac{1}{2}} \right) \right]$$

$$K_r^+ = \frac{224}{\pi^5}\left(\frac{t_r}{h_c}\right)^3 \left(\frac{G_{xz}^{core}}{G_{xy}^{core}}\right)^{\frac{1}{2}} \sum_{p=1,2,3,..}^{\infty} \left[\frac{(1-(-1)^p)^3}{p^5} \tanh\left(\frac{p\pi h_c^3}{8t_r^3} \left(\frac{G_{xy}^{core}}{G_{xz}^{core}} \right)^{\frac{1}{2}} \right) \right]$$

By considering the shear effect of the core, we have and additional equations

$$\begin{Bmatrix} Q_x \\ Q_y \end{Bmatrix} = \begin{bmatrix} A_{ij} \end{bmatrix} \begin{Bmatrix} \phi_x \\ \phi_y \end{Bmatrix} + \begin{bmatrix} D_{ij} \end{bmatrix} \begin{Bmatrix} \phi_x^* \\ \phi_y^* \end{Bmatrix} \tag{25}$$

$$\begin{Bmatrix} Q_x^* \\ Q_y^* \end{Bmatrix} = \begin{bmatrix} D_{ij} \end{bmatrix} \begin{Bmatrix} \phi_x \\ \phi_y \end{Bmatrix} + \begin{bmatrix} F_{ij} \end{bmatrix} \begin{Bmatrix} \phi_x^* \\ \phi_y^* \end{Bmatrix} \tag{26}$$

$$\begin{Bmatrix} S_x \\ S_y \end{Bmatrix} = \begin{bmatrix} D_{ij} \end{bmatrix} \begin{Bmatrix} k_{xz} \\ k_{yz} \end{Bmatrix} \tag{27}$$

Where *i, j= 4,5*.

Where $[A_{ij}]$, $[D_{ij}]$ and $[F_{ij}]$ are the shear stiffnesses matrix of the sandwich core given by

$$\begin{bmatrix} A_{44} & A_{45} \\ A_{45} & A_{55} \end{bmatrix} = \begin{bmatrix} \dfrac{G_{yz} h_c t_r}{L_x} & 0 \\ 0 & \dfrac{G_{xz} h_c t_s}{L_y} \end{bmatrix}^{core} \tag{28}$$

$$\begin{bmatrix} D_{44} & D_{45} \\ D_{45} & D_{55} \end{bmatrix} = \begin{bmatrix} \dfrac{G_{yz} h_c^3 t_r}{12 L_x} & 0 \\ 0 & \dfrac{G_{xz} h_c^3 t_s}{12 L_y} \end{bmatrix}^{core} \tag{29}$$

$$\begin{bmatrix} F_{44} & F_{45} \\ F_{45} & F_{55} \end{bmatrix} = \begin{bmatrix} \dfrac{G_{yz} h_c^5 t_r}{80 L_x} & 0 \\ 0 & \dfrac{G_{xz} h_c^5 t_s}{80 L_y} \end{bmatrix}^{core} \tag{30}$$

The resultants in Eqs. (6)-(30) can be related to the total strain by the following equations

$$\begin{Bmatrix} N_x \\ N_y \\ N_x^* \\ N_y^* \\ M_x \\ M_y \\ M_x^* \\ M_y^* \end{Bmatrix} = \begin{bmatrix} A_s \end{bmatrix} \begin{Bmatrix} \varepsilon_{x0} \\ \varepsilon_{y0} \\ \varepsilon_{x0}^* \\ \varepsilon_{y0}^* \\ k_x \\ k_y \\ k_x^* \\ k_y^* \end{Bmatrix} + \begin{bmatrix} A_s^{'} \end{bmatrix} \begin{Bmatrix} \varepsilon_{xy0} \\ \varepsilon_{xy0}^* \\ k_{xy} \\ k_{xy}^* \end{Bmatrix} \tag{31}$$

$$\begin{Bmatrix} N_{xy} \\ N_{xy}^* \\ M_{xy} \\ M_{xy}^* \end{Bmatrix} = \begin{bmatrix} B_s^{'} \end{bmatrix} \begin{Bmatrix} \varepsilon_{x0} \\ \varepsilon_{y0} \\ \varepsilon_{x0}^* \\ \varepsilon_{y0}^* \\ k_x \\ k_y \\ k_x^* \\ k_y^* \end{Bmatrix} + \begin{bmatrix} B_s \end{bmatrix} \begin{Bmatrix} \varepsilon_{xy0} \\ \varepsilon_{xy0}^* \\ k_{xy} \\ k_{xy}^* \end{Bmatrix} \tag{32}$$

$$\begin{Bmatrix} Q_x \\ Q_x^* \\ S_x \end{Bmatrix} = \begin{bmatrix} D_s \end{bmatrix} \begin{Bmatrix} \phi_x \\ \phi_x^* \\ k_{xz} \end{Bmatrix} + \begin{bmatrix} D_s^{'} \end{bmatrix} \begin{Bmatrix} \phi_y \\ \phi_y^* \\ k_{yz} \end{Bmatrix} \tag{33}$$

$$\begin{Bmatrix} Q_y \\ Q_y^* \\ S_y \end{Bmatrix} = \begin{bmatrix} E_s^{'} \end{bmatrix} \begin{Bmatrix} \phi_x \\ \phi_x^* \\ k_{xz} \end{Bmatrix} + \begin{bmatrix} E_s \end{bmatrix} \begin{Bmatrix} \phi_y \\ \phi_y^* \\ k_{yz} \end{Bmatrix} \tag{34}$$

Where $[A_s]$, $[A_s^{'}]$, $[B_s]$, $[B_s^{'}]$, $[D_s]$, $[D_s^{'}]$, $[E_s]$, $[E_s^{'}]$ are the global stiffnesses matrix of orthogrid the sandwich panel. Stiffnesses matrices are obtained by algebraic sum of both skins and stiffeners rigidity contribution. For symmetric sandwich panel $[A_s^{'}]$, $[B_s^{'}]$, $[D_s^{'}]$, $[E_s^{'}]$ are zero. But $[A_s]$, $[B_s]$, $[D_s]$, $[E_s]$ are given by

$$\begin{bmatrix} A_s \end{bmatrix} = \sum_{L=1}^{NL} \begin{bmatrix} A_{11} & A_{12} & A_{11}^* & A_{12}^* & B_{11} & B_{12} & E_{11} & E_{12} \\ A_{21} & A_{22} & A_{12}^* & A_{22}^* & B_{21} & B_{22} & E_{21} & E_{22} \\ A_{11}^* & A_{12}^* & A_{11}^{**} & A_{12}^{**} & E_{11} & E_{12} & G_{11} & G_{12} \\ A_{12}^* & A_{22}^* & A_{12}^{**} & A_{22}^{**} & E_{21} & E_{22} & G_{21} & G_{22} \\ B_{11} & B_{12} & E_{11} & E_{12} & D_{11} & D_{12} & F_{11} & F_{12} \\ B_{21} & B_{22} & E_{21} & E_{22} & D_{21} & D_{22} & F_{21} & F_{22} \\ E_{11} & E_{12} & G_{11} & G_{12} & F_{11} & F_{12} & H_{11} & H_{12} \\ E_{21} & E_{22} & G_{21} & G_{22} & F_{21} & F_{22} & H_{21} & H_{22} \end{bmatrix} \tag{35}$$

$$\begin{bmatrix} B_S \end{bmatrix} = \sum_{L=1}^{NL} \begin{bmatrix} A_{66} & A_{66}^* & B_{66} & E_{66} \\ A_{66}^* & A_{66}^{**} & E_{66} & G_{66} \\ B_{66} & E_{66} & D_{66} & F_{66} \\ E_{66} & G_{66} & F_{66} & H_{66} \end{bmatrix} \tag{36}$$

$$\begin{bmatrix} D_s \end{bmatrix} = \begin{bmatrix} A_{44} & 3D_{44} & 0 \\ D_{44} & 3F_{44} & 0 \\ 0 & 0 & 2D_{44} \end{bmatrix} \tag{37}$$

$$\begin{bmatrix} E_s \end{bmatrix} = \begin{bmatrix} A_{55} & 3D_{55} & 0 \\ D_{55} & 3F_{55} & 0 \\ 0 & 0 & 2D_{55} \end{bmatrix} \tag{38}$$

2.2 Equation of motion

The governing equations for the free vibration of sandwich panel with orthogonally rib-stiffened core are derived using the HSDT. By using Hamilton's principle, equations of equilibrium for the dynamic analysis of the sandwich plate are obtained using the Hamilton's principle. For the free vibration, the variational principle can be written as

$$\delta \int_{t_1}^{t_2} \left[K - \left(U + V \right) \right] dt = 0 \tag{39}$$

where U is the total strain energy due to deformation, V is the potential of the external loads, and $U+V=\Pi$ is the total potential energy and K is the kinematic energy of the system. δ denotes the

variational symbol. Substituting energy expressions into the Hamilton's principle, the following relation is obtained (Kant and Swaminathan 2001)

$$\begin{aligned} 0 = -\int_0^t \left[\int_{-\frac{H}{2}}^{\frac{H}{2}} \int_A \left(\sigma_x \delta\varepsilon_x + \sigma_y \delta\varepsilon_y + \tau_{xy}\delta\gamma_{xy} + \tau_{yz}\delta\gamma_{yz} + \tau_{xz}\delta\gamma_{xz} \right) dA dz \right] dt \\ + \frac{\delta}{2} \int_0^t \int_{-\frac{H}{2}}^{\frac{H}{2}} \int_A \rho \left[\left(\dot{u} \right)^2 + \left(\dot{v} \right)^2 + \left(\dot{w} \right)^2 \right] dA dz dt \end{aligned} \tag{40}$$

Substituting Eqs. (2), (3) and (4) in Eq. (40), integrating expressions (11) by parts to relieve the virtual generalized displacements δu_0, δv_0, δw_0, $\delta\theta_x$, $\delta\theta_y$, δu_0^*, δv_0^*, $\delta\theta_x^*$ and $\delta\theta_y^*$ of any differentiation and using the fundamental lemma of calculus of variations, we get the following Euler-Lagrange equations (Reddy 1984)

$$\begin{aligned} \delta u_0 : \frac{\partial N_x}{\partial x} + \frac{\partial N_{xy}}{\partial y} &= I_1 \ddot{u}_0 + I_2 \ddot{\theta}_x + I_3 \ddot{u}_0^* + I_4 \ddot{\theta}_x^*, \\ \delta v_0 : \frac{\partial N_y}{\partial y} + \frac{\partial N_{xy}}{\partial x} &= I_1 \ddot{v}_0 + I_2 \ddot{\theta}_y + I_3 \ddot{v}_0^* + I_4 \ddot{\theta}_y^*, \\ \delta w_0 : \frac{\partial Q_x}{\partial x} + \frac{\partial Q_y}{\partial y} = I_1 \ddot{w}_0,\ \delta\theta_x : \frac{\partial M_x}{\partial x} + \frac{\partial M_{xy}}{\partial y} - Q_x &= I_2 \ddot{u}_0 + J_3 \ddot{\theta}_x + I_4 \ddot{u}_0^* + J_5 \ddot{\theta}_x^*, \\ \delta\theta_y : \frac{\partial M_y}{\partial y} + \frac{\partial M_{xy}}{\partial x} - Q_y &= I_2 \ddot{v}_0 + J_3 \ddot{\theta}_y + I_4 \ddot{v}_0^* + J_5 \ddot{\theta}_y^*, \\ \delta u_0^* : \frac{\partial N_x^*}{\partial x} + \frac{\partial N_{xy}^*}{\partial y} - 2S_x &= I_3 \ddot{u}_0 + I_4 \ddot{\theta}_x + I_5 \ddot{u}_0^* + I_6 \ddot{\theta}_x^*, \\ \delta v_0^* : \frac{\partial N_y^*}{\partial y} + \frac{\partial N_{xy}^*}{\partial x} - 2S_y &= I_3 \ddot{v}_0 + I_4 \ddot{\theta}_y + I_5 \ddot{v}_0^* + I_6 \ddot{\theta}_y^*, \\ \delta\theta_x^* : \frac{\partial M_x^*}{\partial x} + \frac{\partial M_{xy}^*}{\partial y} - 3Q_x^* &= I_4 \ddot{u}_0 + J_5 \ddot{\theta}_x + I_6 \ddot{u}_0^* + J_7 \ddot{\theta}_x^*, \\ \delta\theta_y^* : \frac{\partial M_y^*}{\partial y} + \frac{\partial M_{xy}^*}{\partial x} - 3Q_y^* &= I_4 \ddot{v}_0 + J_5 \ddot{\theta}_y + I_6 \ddot{v}_0^* + J_7 \ddot{\theta}_y^*, \end{aligned} \tag{41}$$

Further, I_i, i=1,7 are the mass moments of inertia, given by

$$I_1, I_2, I_3, I_4, I_5, I_6, I_7 = \int_{H_2}^{H_1} \rho_i \left(1, z, z^2, z^3, z^4, z^5, z^6\right) dz \tag{42}$$

Where ρ_i combines the densities of skins ρ_1 and the core ρ_2. For the integration limits, $H_1 = \pm h_s/2 \pm h$ and $H_2 = \pm h_s/2$ for the skins, while $H_1 = h_s/2$ and $H_2 = -h_s/2$ for the core.
And the torsional moment of the core is given by Leknitskii (1981), Reddy (1984)

$$J_i = \rho_{core} \left(\frac{J_{is}}{4L_y} + \frac{J_{ir}}{4L_x} \right); i = 3,5,7 \tag{43}$$

Where J_{is} and J_{ir} are the torsional moment of the stringers and the ribs respectively

$$J_{3s,r} = h_c t_{s,r}^3 \left[\frac{1}{3} - \frac{96}{\pi^5} \frac{t_{s,r}}{h_c} \sum_{p=1,2,3,..}^{\infty} \left[\frac{1-(-1)^p}{p^5} \tanh\left(\frac{p\pi h_c}{2t_{s,r}} \right) \right] \right]$$

$$J_{5s,r} = h_c t_{s,r}^5 \left[\frac{1}{5} - \frac{64}{\pi^5} \left(\frac{t_{s,r}}{h_c} \right)^2 \sum_{p=1,2,3,..}^{\infty} \left[\frac{1-(-1)^p}{p^5} \tanh\left(\frac{p\pi h_c^2}{4t_{s,r}^2} \right) \right] \right]$$
$$J_{7s,r} = h_c t_{s,r}^7 \left[\frac{1}{7} - \frac{128}{\pi^5} \left(\frac{t_{s,r}}{h_c} \right)^3 \sum_{p=1,2,3,..}^{\infty} \left[\frac{1-(-1)^p}{p^5} \tanh\left(\frac{p\pi h_c^3}{8t_{s,r}^3} \right) \right] \right] \quad (44)$$

For simply supported boundaries conditions on the fouredges, we used:
At edges $x=0$ and $x=a$

$$\boldsymbol{v}_0 = \mathbf{0},\ w_0 = 0,\ \theta_y = 0,\ M_x = 0,\ v_0^* = 0,\ \theta_y^* = 0,\ M_x^* = 0,\ N_x = 0,\ N_x^* = 0 \quad (45)$$

At edges $y=0$ and $y=b$

$$\boldsymbol{u}_0 = \mathbf{0},\ w_0 = 0,\ \theta_x = 0,\ M_y = 0,\ u_0^* = 0,\ \theta_x^* = 0,\ M_y^* = 0,\ N_y = 0,\ N_y^* = 0 \quad (46)$$

Following Navier's solution procedure, the solution to the displacement variables satisfying the proposed boundary conditions can be expressed in the following forms

$$u_0 = \sum_{m=1}^{\infty}\sum_{n=1}^{\infty} u_{0mn} \cos\alpha x \sin\beta y e^{-i\omega t}$$
$$v_0 = \sum_{m=1}^{\infty}\sum_{n=1}^{\infty} v_{0mn} \sin\alpha x \cos\beta y e^{-i\omega t}$$
$$w_0 = \sum_{m=1}^{\infty}\sum_{n=1}^{\infty} w_{0mn} \sin\alpha x \sin\beta y e^{-i\omega t}$$
$$\theta_x = \sum_{m=1}^{\infty}\sum_{n=1}^{\infty} \theta_{xmn} \cos\alpha x \sin\beta y e^{-i\omega t}$$
$$\theta_y = \sum_{m=1}^{\infty}\sum_{n=1}^{\infty} \theta_{ymn} \sin\alpha x \cos\beta y e^{-i\omega t} \quad (47)$$
$$u_0^* = \sum_{m=1}^{\infty}\sum_{n=1}^{\infty} u_{0mn}^* \cos\alpha x \sin\beta y e^{-i\omega t}$$
$$v_0^* = \sum_{m=1}^{\infty}\sum_{n=1}^{\infty} v_{0mn}^* \sin\alpha x \cos\beta y e^{-i\omega t}$$
$$\theta_x^* = \sum_{m=1}^{\infty}\sum_{n=1}^{\infty} \theta_{xmn}^* \cos\alpha x \sin\beta y e^{-i\omega t}$$
$$\theta_y^* = \sum_{m=1}^{\infty}\sum_{n=1}^{\infty} \theta_{ymn}^* \sin\alpha x \cos\beta y e^{-i\omega t}$$

Where $\alpha = \frac{m\pi}{a}$ and $\beta = \frac{n\pi}{b}$ and where ω is the natural frequency of the system for any value of m and n.

The substitution of Eq. (46) in Eq. (41), considering all boundary conditions and collecting the coefficients, we obtain finally

$$\left([K]-\omega^2[M]\right)\begin{Bmatrix} u_0 \\ v_0 \\ w_0 \\ \theta_x \\ \theta_y \\ u_0^* \\ v_0^* \\ \theta_x^* \\ \theta_y^* \end{Bmatrix} = \{0\} \tag{48}$$

The matrix [K] refers to global stiffness matrix. In our case, this matrix was directly calculated by a MATLAB program due to complexity caused by the orthogrid stiffeners. On the other hand, it can be analyzed analytically for simple core, like reference (Kant and Swaminathan 2001). Since we have an orthogonally rib-stiffened sandwich panel, the mass matrix [M] has been partially modified from that of reference. Where, these parameters are given by

$$\begin{gathered} M_{8,3}=M_{8,5}=M_{8,7}=M_{8,9}=0, \\ M_{9,1}=M_{9,3}=M_{9,4}=M_{9,6}=M_{9,8}=0, \end{gathered} \quad M_{1,1}=M_{2,2}=M_{3,3}=I_1,$$

$$M_{1,4}=M_{2,5}=M_{4,1}=M_{5,2}=I_2,\ M_{1,6}=M_{2,7}=M_{6,1}=M_{7,2}=I_3,\ M_{4,4}=M_{5,5}=J_3,$$

$$\begin{gathered} M_{1,8}=M_{2,9}=M_{4,6}=M_{5,7}=I_4, \\ M_{6,4}=M_{7,5}=M_{8,1}=M_{9,2}=I_4, \end{gathered} \quad M_{4,8}=M_{5,9}=M_{8,4}=M_{9,5}=J_5,\ M_{6,6}=M_{7,7}=I_5, \tag{49}$$

$$M_{6,8}=M_{7,9}=M_{8,6}=M_{9,7}=I_6,\ M_{8,8}=M_{9,9}=J_7,$$

It should be noted that not cited masses are zero.

2.3 Validation of the analytical model

As there are no applications available on the vibration behavior of a partially bio-based sandwich panel (Alfa fibers) with an orthogonally ribbed core, the validation of the present model was made only with a graphite/epoxy sandwich panel. In order to evaluate the current model, the comparison was made with the results of the literature giving the nondimensionalized natural frequency $\bar{\omega}$ of a simply supported sandwich panels. Mechanical properties both sheets of the antisymmetric (0/90/core/0/90) sandwich panel are given in Table 1.

For this validation, the variation of natural frequency versus side-to-thickness ratio *(a/H)* and equivalent thickness of the core to thickness of the face *(h_s/h)* of the sandwich with antisymmetric (0/90/core/0/90) cross-ply faces was considered. The validation was made with the HSDT (Kant

Table 1 Mechanical properties of isotropic core and Graphite-Epoxy T300/934 face sheets [6]

Materials	E_1 (GPa)	E_2=E_3 (GPa)	G_{12} (GPa)	G_{13}=G_{23} (GPa)	υ_{12}=υ_{13}	υ_{23}	ρ (kg/ m^3)
Face sheets	131	6.895	6.895	6.205	0.22	0.49	1627
Core	6.89×10^{-3}	6.89×10^{-3}	3.45×10^{-3}	3.45×10^{-3}	*0*	0	97

Table 2 The nondimensionalized natural frequency $\bar{\omega} = (\omega b^2/H)\sqrt{(\rho/E_2)_f}$ with a/b=1 and h_s/h=10

a/H	Present Model	Kant and Swaminathan (2001)	Reddy (1984, 2003)
4	2.0944	2.0950	3.1013
10	4.8589	4.8590	7.0473
20	8.5920	8.5920	11.2664
50	13.6603	13.6603	15.0323
100	15.3537	15.3537	15.9522

Table 3 The nondimensionalized natural frequency $\bar{\omega} = (\omega b^2/H)\sqrt{(\rho/E_2)_f}$ with a/b=1 and a/H=10

h_s/h	Present Model	Kant and Swaminathan (2001)	Reddy (1984, 2003)
4	9.1237	9.1238	10.7409
10	4.8593	4.8590	7.0473
20	2.9186	2.9183	4.3734
50	2.3991	2.4004	3.0561
100	2.5182	2.5180	3.0500

(a) (b) (c)

Fig. 4 Alfa fibers (a) the Alfa plant, (b) the Alfa bundles, (c) crushed and sieved Alfa fibers

and Swaminathan model 2011) and a higher order theory of Reddy (1984). From Tables 2 and 3, it is clear that the present model is in perfect accordance this Kant and Swaminathan model (Kant and Swaminathan 2011). But a notable difference is observed with the Reddy model (Reddy 1984) because the effect of transverse normal deformation is not considered. This difference does not exceed 30% for a/H ratio and 15% for h_s/h ratio. This difference becomes very small for high geometric ratios (3.7% for a/H *and* 17% for h_s/h), where the effect of the high order becomes insignificant.

3. Experimental model

3.1 Alfa fiber and Resin

Alfa fibers used as reinforcement for the bio-composite sandwich structure (Fig. 4(a)), were collected from region of Djelfa (Semi-arid center region of Algeria). To have the short Alfa fibers,

we followed the same technique used by Hamammousse *et al*. (2019), Amrane *et al*. (2019). Where, stems were separated and dried with ambient air. Firstly, the soil, roots, dust and all other impurities were removed. Manually, stems were cut into bundles of 3-5 cm (Fig. 4(b)) and crushed with electric grinder equipped with three sets of hammers blade. The short fibers were separated from the powder by sieving (Fig. 4(c)).

An epoxy resin is used to fabricate the material of composite sandwich panel. Medapoxy STR furnished from Granitex Company (Granitex, Oued Smar, Algiers, Algeria) was obtained by mixing 60% of resin and 40 of hardener. The polymerization of the composite is on term of 17 days at ambient temperature. Finally, a post-curing of specimens was accomplished treatment for 8h at 80° to obtain the maximum mechanical strength and stability. The density of the resin was specified by the manufacturer as (1.1+0.005) g/cm^3.

3.2 Tensile test

The tensile test specimens by impregnating Alfa fibers at different mass fractions (i.e., 5%, 10%, 15% and 20%) in Medapoxy STR resin. To have perfect specimen edges, samples were cut by a laser machine (Trotec Speedy400). Tensile tests were made on an Instron universal machine of 5 kN capacity with displacement of 1mm/min, corresponding to a strain rate of 10^{-4}1/s. Two strain gauges were fixed to measure the longitudinal and transverse strains. For each specimen, density, Young's modulus, Poisson's ratio, and ultimate strain and stress were predicted. Three specimens for each mass fraction were tested. For a better representation, only stress-strain curves of the composite with 5% of Alfa fiber were plotted in Fig. 5. The main properties of the other cases are relisted in Table 2. We observed typical stress-strain curves. For small loads, all curves exhibited a linear behavior. With the increase of the load its behavior becomes more and more nonlinear until the total rupture of the specimens. Due to the variation in the short fiber length, diameter and orientation, a small dispersion was observed for each curve. This dispersion was confirmed by similar tests reported in literature (Marrakchi *et al*. 2011). In addition, effect of form factor and mass fraction of Alfa short fibers effect was given in Table 1 of Amrane *et al*. (2019). But effect of fibers treatment was given by Adjal *et al*. (2021). In both papers, we concluded that, fibers are 0.1 mm to 0.5 mm in diameter and 0.86 mm to 4.5 mm in length.

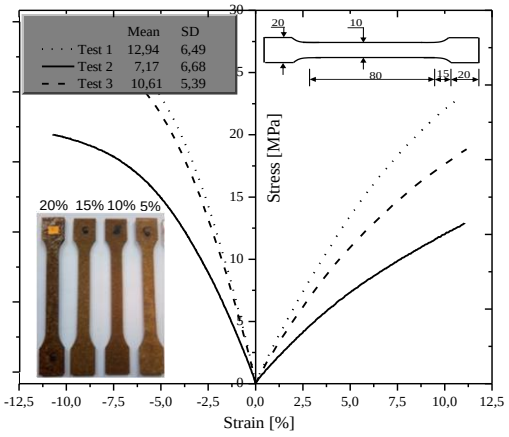

Fig. 5 Typical stress-strain curves of the composite with 5% of Alfa fiber

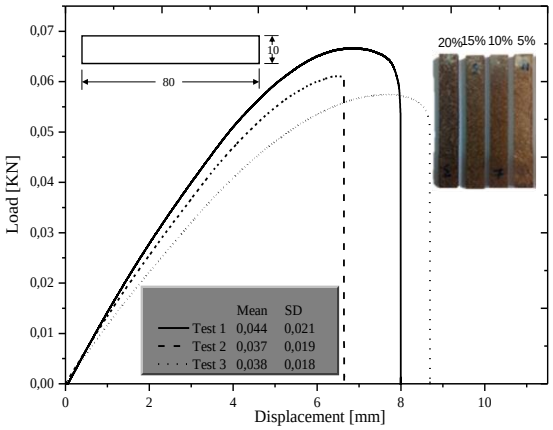

Fig. 6 Typical force-displacement of bending of the composite with 5% of Alfa fiber

3.3 Bending test

The bending specimens were designed according to the ASTM D790 (Fig. 6). The specimens were also cut using a laser machine (Trotec Speedy 400). The specimens were then measured and weighed using high-precision measuring tools. The density of the different composite mass fraction was obtained. After that, the three points bending tests were performed on an MTS 43 universal machine of 5 kN cell equipped with an indenter hemispherical head. Due to the random distribution of the short fibers within the matrix, three specimens for each mass fraction were made. The typical curves of force-displacement of bending tests for partially bio-sourced specimens (5% of shorts fibers content) are shown in Fig. 6. It is clear that in spite of this remarkable dispersion caused certainly by the fibers arrangement diameters, all curves take the same shape. A linear behavior was observed for the small loads, followed by a nonlinear response with an increasing load displacement until the abrupt rupture of the specimen. From each fibers content, values of Young's modulus, ultimate stress and strain are deduced and gathered in the table 4. We observed that the fiber volume fraction clearly affected material rigidity. Almost all the mechanical characteristics were ameliorated by increasing the Alfa fibers content until 10%. Beyond this fibers content, we noticed a rather remarkable drop in both tensile and bending mechanical properties except the ultimate strain.

The volume fraction of Alfa fibers was limited to 20%, because we found from the above works (Hamamousse *et al*. 2019, Amrane *et al*. 2019) as well as the work cited in the literature (Zaman *et al*. 2011), that beyond the mass fraction of 10%, we have a reduction in the mechanical characteristics of the bio-sourced composite. This decrease is due to poor interfacial bonding between fibers and matrix caused incompatibility between both natures of epoxy matrix (hydrophobic) and fibers natural (hydrophilic) which behave like voids in the continuous phase. Because of the discontinuity, the irregularity, the random orientation and diameters variation of fibers, stress transfer in short-fiber composites becomes relatively inefficient between the fibers and the matrix. However, this behavior allows for a more flexible structure caused by the increase in ultimate strain versus the fiber content. The brittleness of the fibers also contributed to low mechanical strength as scientific fibers contain higher possibilities for the fibers to transmit higher loads. This conclusion was confirmed by some papers cited in literature (Djoudia *et al*. 2019, Shah *et al*. 2019, Li *et al*. 2007).

Table 4 Mechanical properties of the tested composites

Test	Fiber mass fraction (%)	Density (g/cm^3)	Young's modulus E (GPa)	Poisson's Ratio υ	Ultimate stress (MPa) σ^u	Ultimate strain (%) ε^u
Tensile	5%	1.498	2.75 ± 0.07	0.37±0.03	32.47 ± 4.41	1.52 ± 0.31
	10%	1.253	3.06 ± 0.07	0.39±0.01	22.39 ± 9.49	0.91 ± 0.42
	15%	1.152	2.51 ± 0.19	0.35±0.06	22.33 ± 0.94	1.34 ± 0.12
	20%	1.078	2.19 ± 0.63	0.34±0.27	12.88 ± 5.41	0.73 ± 0.34
Bending	5%	1.498	2.39 ± 0.09	--	55.60 ± 1.43	3.36 ± 0.27
	10%	1.253	2.57 ± 0.19	--	53.35 ± 3.37	2.73 ± 0.33
	15%	1.152	2.28 ± 0.15	--	40.77 ± 3.35	2.59 ± 0.11
	20%	1.078	1.50 ± 0.67	--	29.54 ± 9.48	3.24 ± 1.05

(a) The aluminum mold (200×200 mm)

(b) The molded sandwich panel with 60 grid points used to capture the mode shapes

Fig. 7 The sandwich plate specimens

3.3 Free vibration tests

For the vibration tests, sandwich plates with orthogrid core with different mass fractions were molded using an aluminum mold (Fig. 7(a)). The stiffened orthogrid panels were cast in an aluminum mold with two different faces. In the unstiffened face, we machined a square plate 200 mm×200 mm with 3 mm deep. On the other hand, the stiffened face was obtained by machining the square plate followed by machining of orthogrid (6 mm deep) with a spacing of 60mm between stiffeners in both directions. After molding and polymerization, both faces were attached to each other by a rigid adhesive under pressure applied by a hydraulic press during 24 hours. The plates have a square external shape with an area of 200 mm×200 mm; the orthogrid design is regular with a spacing of 60mm between stiffeners in both directions (Fig. 7(b)). The average thicknesses of both faces and stiffeners forming the core were (3.01±0.26) mm and (6±0.12) mm, respectively. The slight differences in thickness between the panels are due to the manual molding process in open mold. The mass fractions used are 0%, 5%, 10% and 15%.

A series of free vibration tests were subjected to obtain the natural frequencies and the mode shapes of the rectangular sandwich panels with different mass fractions (5%, 10% and 15%). The sandwich plate was simply supported on the four edges using a metal holder (Fig. 8). Considerable time has been devoted to the manufacture of an adequate dispositive which will allow us to have

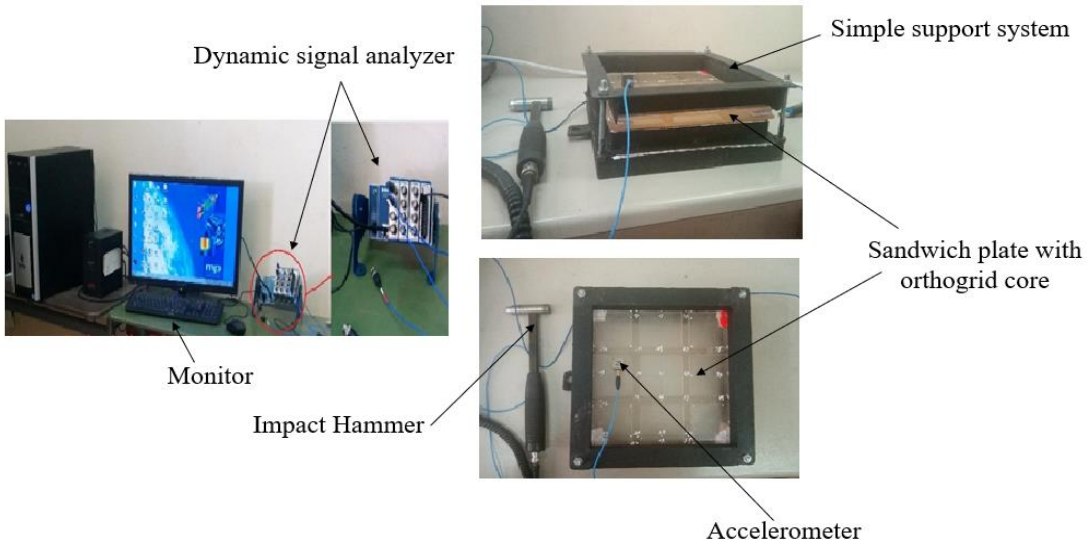

Fig. 8 Basic measurement chain of the natural frequencies of the orthogrid sandwich panel

only simply supported boundary conditions to the contours. Because tightening at the extremities gives us a fixed boundary conditions and relaxation brings us to free boundary conditions. The consequences of these two constraints, give us, in the majority erroneous results due to the associated natural frequencies and mode shapes.

To measure the natural frequencies of the panel, a basic measurement chain composed of transducers, amplifiers, excitation instruments and a fast Fourier transform (FFT) analyzer has been set in Fig. 8. At each gap point, the panel was excited by one of the most common and successfully used methods, i.e., instrumented impact hammer with sensitivity of 2.25 mV. The frequency range was fixed between 0.1 and 2000 Hz. The panel response was sensed by attaching a miniature accelerometer to a predetermined DOF on the orthogrid panel. After that, the excitation by forceinput to the panel and the associated response was measured. According to the change of behavior on the plates, the response auto-spectrum, and the cross spectrum relating these two, the individual FRFs were accordingly evaluated. Only good impact was selected, because it gives a coherence graph that must be near to unity over the full frequency range. In addition, the frequency response functions for each fiber fraction were averaged tree times before transferring to the PC for analysis by maintaining only an acceptable coherence function value.

The vibration response of the sandwich plate with different mass fractions is plotted in Fig. 9. In the fixed frequency range between 0.1 and 2000 Hz, we obtained only three natural frequencies and their mode shapes. We say that the fibers content has an effect on the natural frequencies of the bio-composite sandwich plate. It is obvious that the increase in the Alfa fibers content have a positive effect on the vibration behavior of the sandwich panels. Because, the increase in the fiber content, generates the natural frequencies increase until 10%. This will certainly have an effect on the delay of the resonance pairing. Beyond this percentage, the natural frequencies have been considerably reduced.

To prove the validity and the efficiency of both analytical and experimental analysis, three natural frequencies for each case representing fiber contents are given in Table 5. From this table, we note that analytical and experimental results are in good agreement with rather negligible errors.

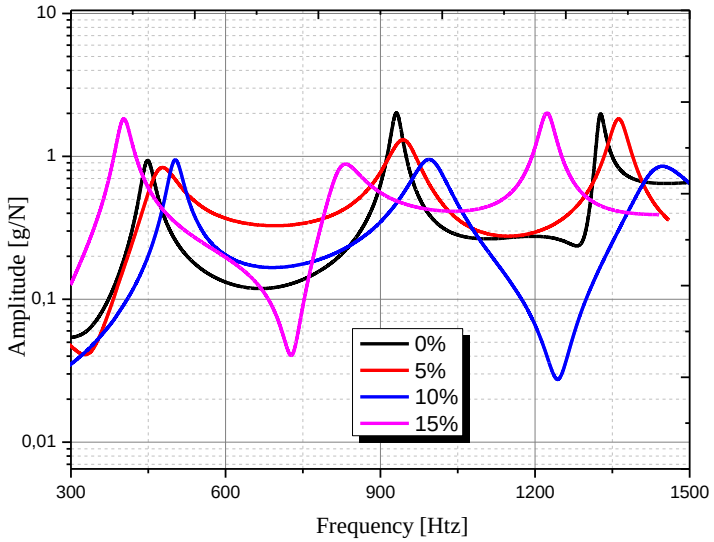

Fig. 9 Natural frequencies of the sandwich plate simply supported

Table 5 Experimental and analytical natural frequencies versus fibers content

Fibers content	0%			5%			10%			15%		
	Exp.	Ana.	Dif(%)	Exp.	Ana.	Dif (%)	Exp.	Ana.	Dif (%)	Exp.	Ana.	Dif (%)
1st Freq	448.8	451.4	0.60	475.1	475.8	0.15	500.2	495.6	0.93	402.7	404.8	0.54
2nd Freq	931.3	931.7	0.04	945.8	966.2	2.11	994.9	995.2	0.03	831.5	824.4	0.86
3rd Freq	1327.7	1319.1	0.65	1360.	1363.	0.26	1447.7	1405.5	2.90	1222	1164	4.98

analytical results were slightly superior to those of the experimental model. This discrepancy might be caused generally by the damping effect, the additional mass of the accelerometer, the experimental boundary conditions which are weaker than the simply supported boundary conditions considered in the analytical model. Another effect can be significant; it is about the arrangement of the fibers within the matrix which is random. The maximum relative error is less than 0.93% for the first natural frequency and 4.98% for the third frequency. In practice, the prediction accuracy of the first frequency is often the most interesting since the link with the minimum level of energy resonances begins to emerge, is very high. From the second frequency, a minor but fairly common underestimation of the natural frequencies also seems evident.

It is obvious that according to the developed analytical model, the natural frequencies strongly depend on the rigidity and the mass of the structure. Therefore, an increase in stiffness or a reduction in natural frequency is influenced by these two parameters.

In order to verify the accuracy and applicability of the equivalent plate model based on HSDT for sandwich plate with orthogrid core, a comparison in terms of mode shapes among the experimental data and theoretical results was carried out in Fig 10. This comparison shown that no difference seems to emerge with simulations able to correctly reconstruct the deformation trend, which confirms that the good correlation between both analytical and experimental models.

3.4 Damping coefficient

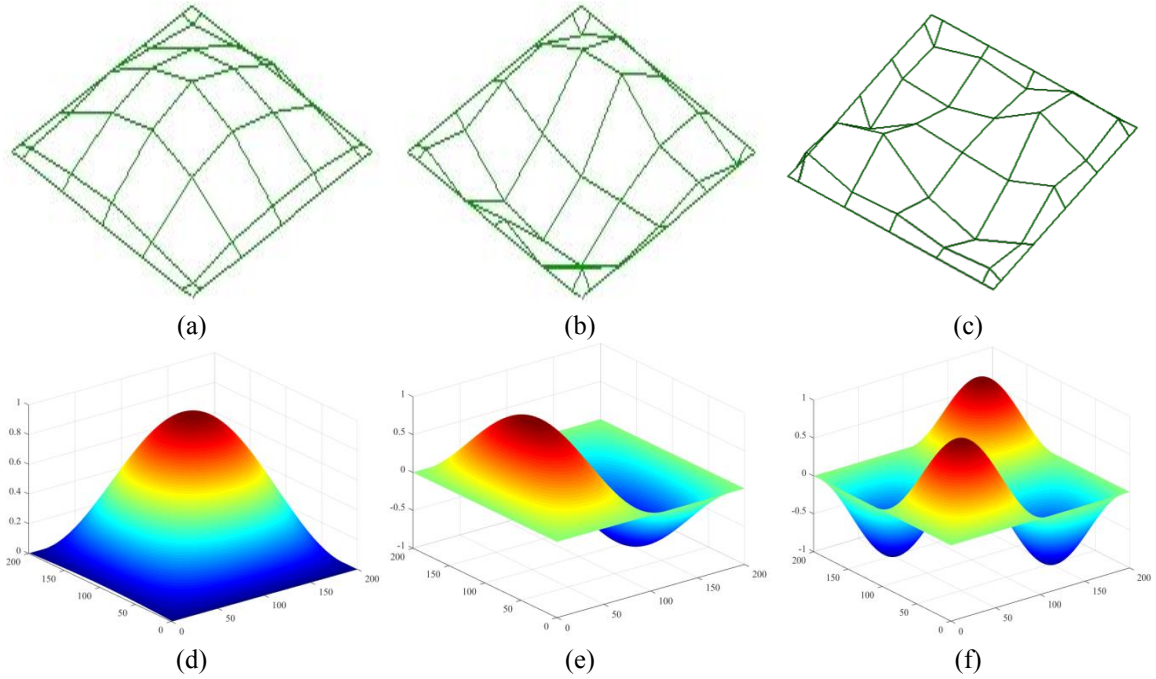

Fig. 10 The third first natural frequencies of the sandwich plate with orthogrid core for 5% of short Alfa fibers. (a), (b) and (c) The three experimental mode shapes. (d), (e) and (f) The three analytical mode shapes

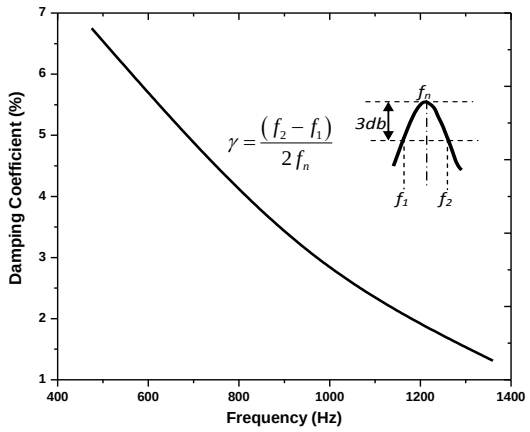

Fig. 11 Damping coefficient versus the frequency for 5% of Alfa Fibers

Compared to metals, the damping of bio-composite materials is almost higher, and is a difficult to predict it, due to the such factors include manufacturing techniques and fiber-matrix bonding. The amplitude response, as shown in Fig. 11, can be used to obtain the damping coefficients. The frequencies f_1 and f_2 are respectively, γf_n below and γf_n above f_n, corresponding a maximum amplitude value. Fig. 11 shows the variation of the damping coefficients as a function of the natural frequencies. The results are obtained for 5% of Alfa fiber. They showed that the damping coefficient of bio-composite beams decreased according to the increase in frequency or mode shape. From

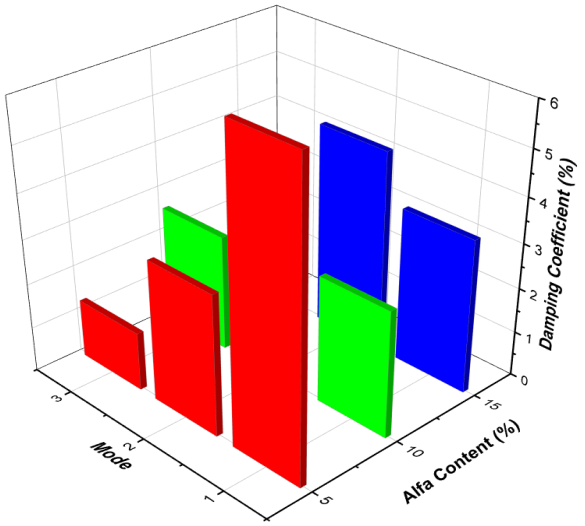

Fig. 12Variation of the damping coefficient versus Alfa content and mode shape.

literature, the damping coefficients of Alfa fiber composite beam are significantly higher than those attributed by carbon fiber and metal structures (Adjal *et al*. 2021, Ben Ameur *et al*. 2018). Fig. 12 shows the 3D bars of the damping coefficients versus Alfa content and mode shapes.In all the cases, the maximum values of the damping coefficient were obtained for the first mode shape. But, it has been intensely reduced with the increase in the fiber content of Alfa.

4. Conclusions

The main objective of this paper was to propose both analytical and experimental models to study the free vibration of sandwich panel with orthogonally stiffened core. For a variable mass fraction of Alfa fibers, static (tensile and bending) and free vibration tests was made to study the behavior of partially bio-sourced sandwich panel. Using simply supported boundary conditions, an experimental test was carried out using an impact hammer for predicting the natural frequencies and the mode shapes of the bio-sourced sandwich panel. After that, an analytical model based on the HSDT was developed to predict fundamental frequencies and the mode shapes according to Navier's solution. On the basis of the experimental and analytical investigation, the conclusions obtained are as follows;

- Tensile tests show typical stress-strain curves attributed to the non-linear behavior of the STR epoxy Resin.
- For the bending test, a linear behavior was observed for the small loads, followed by a nonlinear response with an increasing load displacement until the abrupt rupture of the specimen.
- The validation of the nondimensionalized natural frequencies with the literature showed the efficiency of the analytical model.Where the present model was in perfect agreement with similar HSDT models and in good agreement with FSDT models mainly for high geometric ratios of the sandwich panel.
- We noticed that the non-dimensional naturalfrequencies increased considerably with the side-

to-thickness ratio but decreased with the thickness of the core on the thickness of the flange. This confirms that their vibration behavior was significantly influenced by the geometric and mechanical properties of the Alfa fibers.

• The comparison between the proposed analytical and experimental analysis show good agreement with rather negligible errors caused generally by the by the damping effect, the additional mass of the accelerometer, the experimental boundary conditions and the randomly arrangement of the fibers in the matrix.

• From the series of free vibration tests of the sandwich panels with different content of fibers (5%, 10% and 15%). It is obvious that the increase in the Alfa fibers content have a positive effect on the vibration behavior of the sandwich panels until 10%. Beyond this percentage, the natural frequencies have been considerably reduced because the natural frequencies are strongly dependent on the rigidity and the mass of the sandwich structure. So, the increase or decrease in the natural frequency is influenced by the mass and stiffness of the structure.

• The maximal values of damping coefficient were obtained for the first mode shape. But, it has been intensely reduced with the increase in the fiber content of Alfa.

• Finally, the comparison in terms of mode shapesconfirms that the good correlation between both analytical and experimental models.

References

Adjal, Y., Sereir, Z., Benzidane, R. and Bendada, A. (2021), "Vibration of damaged bio-composite beams reinforced with random short Alfa fibers: Experimental and analytical investigations", *Adv. Aircraft Spacecraft Sci.*, **8**(2), 127-149. https://doi.org/10.12989/aas.2021.8.2.127.

Amrane, A., Sereir, Z., Poilâne, C. and Vivet, A. (2019), "Effect of form factor and mass fraction of alfa short fibers on the mechanical behavior of an Alfa/Green poxy bio-composite", *J. Compos. Adv. Mater.*, **29**(4), 185191. https://doi.org/10.18280/RCMA.290401.

Azarafza, R. (2018), "Fabrication, experimental modal testing, and a numerical analysis of composite sandwich structures with a grid-stiffened core", *Compos. Mater.*, **54**(4), 537-544. https://doi.org/10.1007/s11029-018-9762-4.

Ben Ameur, M., El Mahi, A., Rebiere, J.L., Abdennadher, M. and Haddar, M. (2018), "damping analysis of unidirectional carbon/flax fiber hybrid composites", *Int. J. Appl. Mech.*, **10**(05), 1850050. https://doi.org/10.1142/S1758825118500503.

Benzidane, R., Sereir, Z., Bennegadi, M.L., Doumalin, P. and Poilâne, C. (2018), "Morphology, static and fatigue behavior of a natural UD composite: The date", *Compos. Struct.*, **203**, 110-123. https://doi.org/10.1016/j.compstruct.2018.06.122.

Djoudia, T., Hecinia, M., Scidab, D., Djeblouna, Y. and Djemai, H. (2019), "Physico-mechanical characterization of composite materials based on date palm tree fibers", *J. Nat. Fiber.*, **18**(6), 1-14. https://doi.org/10.1080/15440478.2019.1658251.

Ehsani, A. and Rezaeepazhand, J. (2016), "Vibration and stability of laminated composite orthogrid plates", *J. Reinf. Plast. Compos.*, **35**(13), 1051-1061. https://doi.org/10.1177/0731684416635757.

Fu, T., Chen, Z., Yu, H., Wang, Z. and Liu, X. (2018), "An analytical study of sound transmission through stiffened double laminated composite sandwich plates", *Aerosp. Sci. Tech.*, **82-83**, 92-104. https://doi.org/10.1016/j.ast.2018.09.012.

Halpin, J.C. (1969), *Effects of Environmental Factors on Composite Materials*, Air Force Materials Lab Wright-Patterson AFB OH.

Hamamousse, K., Sereir, Z., Benzidane, R., Gehring, F., Gomina, M. and Poilâne, C. (2019), "Experimental and numerical studies on the low-velocity impact response of orthogrid epoxy panels reinforced with short

plant fibers", *Compos. Struct.*, **211**, 469-480. https://doi.org/10.1016/j.compstruct.2019.01.005.
Jiang, S., Sun, F., Fan, H. and Fang, D. (2017), "Fabrication and testing of composite orthogrid sandwich cylinder", *Compos. Sci. Technol*., **142**, 171-179. https://doi.org/10.1016/j.compscitech.2017.02.009.
Kant, T. and Swaminathan, K. (2001), "Analytical solutions for free vibration of laminated composite and sandwich plates based on a higher order refined theory", *Compos. Struct.*, **53**(1), 73-85. https://doi.org/10.1016/S0263-8223(00)00180-X.
Khaldi, M., Vivet, A., Bourmaud, A., Sereir, Z. and Kada, B. (2016), "Damage analysis of composites reinforced with Alfa fibers: viscoelastic behavior and debonding at the fiber/matrix interface", *J. Appl. Polym. Sci.*, **133**(31), 43760. https://doi.org/10.1002/app.43760.
Leknitskii, S.G. (1981), *Theory of Elasticity of an Anisotropic Body*, Mir Publishers, Moscow.
Li, C., Wu, G., Xiao, F. and Wu, C. (2007), "Damping behavior of sandwich beam laminated with CIIR/petroleum resins blends by DMA measurement", *J. Appl. Polym. Sci.*, **106**(4), 2472-2478. https://doi.org/10.1002/app.25450.
Liu, N. and Jeffers, A.E. (2017), "Isogeometric analysis of laminated composite and functionally graded sandwich plates based on a layerwise displacement theory", *Compos. Struct*., **176**, 143-153. https://doi.org/10.1016/j.compstruct.2017.05.037.
Liu, N. and Jeffers, A.E. (2018), "Adaptive isogeometric analysis in structural frames using a layer-based discretization to model spread of plasticity", *Comput. Struct*., **196**, 1-11. https://doi.org/10.1016/j.compstruc.2017.10.016.
Liu, N., Plucinsky, P. and Jeffers, A.E. (2017), "Combining load-controlled and displacement- controlled algorithms to model thermal-mechanical snap-through instabilities in structures", *J. Eng. Mech*., **143**, 1-11. https://doi.org/10.1061/(ASCE)EM.1943-7889.0001263.
Liu, N., Ren, X. and Lua, J. (2020), "An isogeometric continuum shell element for modeling the nonlinear response of functionally graded material structures", *Compos. Struct*., **237**, 111893. https://doi.org/10.1016/j.compstruct.2020.111893
Marjanović, M., Kolarević, N., Nefovska-Danilović, M. and Petronijević, M. (2016), "Free vibration study of sandwich plates using a family of novel shear deformable dynamic stiffness elements: Limitations and comparison with the finite element solutions", *Thin Wall. Struct.*, **107**, 678-694. https://doi.org/10.1016/j.tws.2016.08.002.
Marrakchi, Z., Khiari, R., Oueslati, H., Mauret, E. and Mhenni, F. (2011), "Pulping and papermaking properties of Tunisian Alfa stems (Stipa tenacissima) effects of refining process", *Ind. Crops. Prod.,* **34**, 1572-1582. https://doi.org/10.1016/j.indcrop.2011.05.022.
Md Shah, A.U., Sultan, M.T. and Jawaid, M. (2019), "Sandwich-structured bamboo powder/glass fibre-reinforced epoxy hybrid composites-Mechanical performance in static and dynamic evaluations", *J. Sandw. Struct. Mater*., **23**(1), 47-64. https://doi.org/10.1016/j.jmrt.2019.09.003.
Merzoug, A., Bouhamida, B., Sereir, Z., Bezazi, A., Kilic, A. and Candan, Z. (2020), "Quasi-static and dynamic mechanical thermal performance of date palm/glass fiber hybrid composites", *J. Ind. Text*., 152808372095803. https://doi.org/10.1177/1528083720958036.
Nemeth, M.P. (2011), "A treatise on equivalent-plate stiffnesses for stiffened laminated-composite plates and plate-like lattices", National Aeronautics and Space Administration, Langley Research Center Hampton, Virginia.
Petrolo, M., Carrera, E., Saeghier, A. and Alawami A.S. (2016), "Free vibration analysis of damaged beams via refined models", *Adv. Aircraft Spacecraft Sci.*, **3**(1), 95-112. http://doi.org/10.12989/aas.2016.3.1.095.
Petrone, G., Carzana, A., Ricci, F. and De Rosa, S. (2017), "Damage detection through structural intensity and vibration based techniques", *Adv. Aircraft Spacecraft Sci.*, **4**(6), 613-637. http://doi.org/10.12989/aas.2017.4.6.613.
Phan, C.N., Frostig, Y. and Kardomateas, G.A. (2013), "Free vibration of unidirectional sandwich panels, Part II: Incompressible core", *J. Sandw. Struct. Mater.*, **15**(4), 412-428. https://doi.org/10.1177/1099636213485520.
Reddy, J.N. (1984), "A simple higher order theory for laminated composite plates", *ASME J. Appl. Mech.*, **51**, 745-752. https://doi.org/10.1115/1.3167719.

Reddy, J.N. (2003), *Mechanics of Laminated Composite Plates and Shells: Theory and Analysis*, Second Edition, CRC Press.

Sahoo, S.S., Panda, S.K. and Singh, V.K. (2017), "Experimental and numerical investigation of static and free vibration responses of woven glass/epoxy laminated composite plate", *J. Mater.: Des. Appl*., **231**(5), 463-478. https://doi.org/10.1177/1464420715600191.

Semmani, A., Sereir, Z. and Hamou, Y. (2020), "Analysis and optimization of composite kagome grid panels subjected to the low velocity impact", *J. Dyn. Behav. Mater.*, **6** 287-302. https://doi.org/10.1007/s40870-020-00243-x.

Shahgholian-Ghahfarokhi, D., Rahimi, G., Zarei, M. and Salehipour, H. (2020), "Free vibration analyses of composite sandwich cylindrical shells with grid cores: experimental study and numerical simulation", *Mech. Bas. Des. Struct. Mach.*, 1-20. https://doi.org/10.1080/15397734.2020.1725565.

Sinha, L., Mishra, S.S., Nayak, A.N. and Sahu, S.K. (2020), "Free vibration characteristics of laminated composite stiffened plates: Experimental and numerical investigation", *Compos. Struct.*, **233**, 11557. https://doi.org/10.1016/j.compstruct.2019.111557.

Teo, S.C., Lan, D.N.U., Teh, P.L. and Tran, L.Q.N. (2016), "Mechanical behavior of palm oil-based composite foam and its sandwich structure with a flax-epoxy composite", *J. Appl. Polym. Sci*., **133**, 43977. https://doi.org/10.1002/app.43977.

Thinh, T.I. and Quoc, T.H. (2010), "Finite element modeling and experimental study on bending and vibration of laminated stiffened glass fiber/polyester composite plates", *Comput. Mater. Sci.*, **49**, S383-S389. https://doi.org/10.1016/j.commatsci.2010.05.011.

Wang, Y. and Wang, X. (2015), "Free vibration analysis of soft-core sandwich beams by the novel weak form quadrature element method", *J. Sandw. Struct. Mater.*, **18**(3), 294-320. https://doi.org/10.1177/1099636215601373.

Whitney, J.M. and Pagano, N.J. (1970), "Shear deformation in heterogeneous anisotropic plates", *ASME J. Appl. Mech.*, **37**(4), 1031-1036.

Xin, F.X. and Lu, T.J. (2011), "Analytical modeling of wave propagation in orthogonally rib-stiffened sandwich structures: Sound radiation", *Comput. Struct.*, **89**, 507-516. https://doi.org/10.1016/j.compstruc.2010.12.007.

Xu, G.D., Zeng, T., Cheng, S., Wang, X.H. and Zhang, K. (2019), "Free vibration of composite sandwich beam with graded corrugated lattice core", *Compos. Struct.*, **229**, 111466. https://doi.org/10.1016/j.compstruct.2019.111466.

Zaman, I., Ismail, A.E. and Awang, M.K. (2011), "Influence of fiber volume fraction on the tensile properties and dynamic characteristics of coconut fiber reinforced composite", *J. Sci. Tech*., **1**(1), 55-71.

Zhang, Z., Li, S. and Huang, Q. (2018), "Low-frequency sound radiation of infinite orthogonally rib-stiffened sandwich structure with periodic subwavelength arrays of shunted piezoelectric patches", *Compos. Struct.*, **187**, 144-156. https://doi.org/10.1016/j.compstruct.2017.12.053.

CC